AIAA 92-0347
Reaction Zone Structure of Weak Underdriven Oblique Detonations

J. M. Powers and K. A. Gonthier
Department of Aerospace and Mechanical Engineering
University of Notre Dame
Notre Dame, Indiana

30th Aerospace Sciences Meeting & Exhibit
January 6-9, 1992 / Reno, NV

REACTION ZONE STRUCTURE OF WEAK UNDERDRIVEN OBLIQUE DETONATIONS

Joseph M. Powers* and Keith A. Gonthier†
Department of Aerospace and Mechanical Engineering
University of Notre Dame
Notre Dame, Indiana 46556

Abstract

Steady weak underdriven oblique detonations consisting of a lead shock attached to a solid wedge followed by a resolved reaction zone structure are admitted as solutions to the reactive Euler equations for eigenvalue shock wave angles. This is demonstrated for a fluid which is taken to be an inviscid, calorically perfect ideal gas which undergoes a two-step irreversible reaction with the first step exothermic and the second step endothermic. These solutions represent two-dimensional extensions of one-dimensional weak detonations. In addition, this model admits solutions to the other two classes of solutions identified by a Rankine-Hugoniot analysis, namely weak overdriven and strong waves. Chapman-Jouguet waves, however, are not admitted. These results contrast those for a corresponding one-step model which, for detonations with a lead shock, only admits weak overdriven, strong, and Chapman-Jouguet solutions.

Introduction

Renewed interest in hypersonic flight has generated interest in devices which employ oblique detonations. An oblique detonation is defined as a combustion process which is induced by an oblique shock. Most recent discussion of oblique detonations has been motivated by the oblique detonation wave engine (ODWE), which has been proposed to propel the National Aerospace Plane (NASP), and the ram accelerator, which has been used to accelerate projectiles to very high speeds.

Figure 1 gives a schematic diagram of the type of oblique detonation to be studied here along with the coordinate system. We consider an incoming unreacted gaseous mixture at supersonic Mach number, $M_o > 1$, which encounters a straight shock, inclined at angle β to the horizontal, which is attached to a curved wedge. The mixture reacts downstream of the shock in the reaction zone. We consider the special case in which the flow has variation in the direction normal to the shock wave, taken to be the x direction as indicated in Fig. 1, but no variation in the direction parallel to the shock, taken to be the y direction. The origin is taken to be the wedge tip. The streamlines are taken to form an angle θ with the horizontal. At complete reaction, θ relaxes to a constant value which we call the wedge angle. The flow has symmetry about the horizontal plane.

Rankine-Hugoniot (RH) analysis has been commonly used to analyze the potential equilibrium states which may be obtained in an oblique detonation. Discussion and analysis are given by Siestrunck, et al.[1], Gross and Chinitz[2], Gross[3], Oppenheim, et al.[4], Chernyi[5], and, more recently, Pratt, et al.[6] The RH analysis allows determination of both β, θ shock and detonation polars. For $M_o = 10$, Fig. 2 shows such polars for an inert oblique shock, $Q = 0$, and an oblique detonation, $Q = 25$, where Q is a dimensionless heat release to be defined later. Following Pratt, et al., we use the final value of the Mach number normal to the shock, M_x, and analogies with inert oblique shock nomenclature to classify oblique detonations. For shock angles below a critical value $\beta < \beta_{CJ}$, there is no real solution to the RH equations. For $\beta = \beta_{CJ}$, there is one solution which corresponds to the Chapman-Jouguet (CJ) solution of one-dimensional theory. For $\beta = \beta_{CJ}$ at complete reaction the normal Mach number is sonic, $M_x = 1$. For $\beta > \beta_{CJ}$, two solutions are obtained. The solution corresponding to the smaller wedge angle has a supersonic normal Mach number, $M_x > 1$ and is known as a weak underdriven solution. Its counterpart with the higher wedge angle is known as a weak overdriven solution if $\beta < \beta_{detach}$ and a strong solution if $\beta \geq \beta_{detach}$. For both weak overdriven and strong solutions, the final normal Mach number is subsonic, $M_x < 1$. Here β_{detach} is the shock angle corresponding to the wedge angle θ_{detach} beyond which there is no attached shock solution. The nomenclature "weak" and "strong" is suggested by

*Assistant Professor, Member AIAA.
†Graduate Assistant.

oblique shock theory and is not consistent with the nomenclature of one-dimensional detonation theory.

The two-dimensional steady flow can be further characterized by the spatially hyperbolic or elliptic character of the governing partial differential equations. With the total Mach number M calculated from the velocity magnitude, the equations are elliptic if $M < 1$ and hyperbolic if $M > 1$. The subsonic to supersonic transition takes place at β_{SS} which is slightly less than β_{detach}. Strong oblique detonations terminate at a subsonic point, $M < 1$. Weak overdriven solutions terminate at either subsonic or supersonic points: for $\beta_{CJ} < \beta < \beta_{SS}$, $M > 1$; for $\beta_{SS} < \beta < \beta_{detach}$, $M < 1$. Generally $\beta_{SS} \sim \beta_{detach}$; consequently the range of weak overdriven solutions with $M < 1$ is very small. Weak underdriven solutions terminate at supersonic points, $M > 1$.

The conditions under which each of these solution classes, each of which satisfies the conservation principles and entropy inequality, could exist in nature is a question which has not been completely answered. A first step is to consider the resolved steady reaction zone structures and examine solution trajectories from an initial state to an equilibrium state in phase space. For a given kinetic scheme, this will disqualify certain classes of solutions. Those that remain should be subjected to the more rigorous test of hydrodynamic stability. What should result is a knowledge of the initial and boundary conditions which are necessary for a solution to exist. Based on analogies with inert theory which show that the existence of a strong or weak oblique shock depends on the downstream boundary conditions, it is hypothesized that there may be boundary conditions for each class of oblique detonation to exist. Given that in the course of its travels, both an ODWE and ram accelerator may encounter boundary conditions suitable for each class of oblique detonation, it stands to reason that each class should be subjected to systematic study.

With this philosophy in mind Powers and Stewart[7] have carried out a study of steady reaction zone structures associated with oblique detonations in which the reaction is one-step and irreversible. With such a kinetic model and for an oblique detonation which includes a straight lead shock, it was shown that the reactive Euler equations admit strong, weak overdriven, and CJ solutions but do not admit weak underdriven solutions.

In the present study, we generalize the model of Ref. 7 to allow for a two-step irreversible reaction with the first step exothermic and the second endothermic. For completeness, we present examples for all three classes of oblique detonations, though our primary purpose is to demonstrate that weak underdriven oblique detonations are admissible. To achieve this end, a particularly simple model is employed which has the same general functional form as models which are commonly used to simulate the combustion of real materials. This model is a two-dimensional extension of a model used by Fickett and Davis[8] (pp. 153-173) to predict one-dimensional weak or eigenvalue detonations. As first suggested in Ref. 7, use of this model leads to a two-dimensional complement of the eigenvalue detonation.

The plan of this paper is as follows. First the model equations are presented. These are reduced to a set of ordinary differential equations by assuming there are no changes in the direction tangent to the shock. Exact expressions are then written for weak overdriven and strong oblique detonations in the hypersonic limit. Away from the hypersonic limit, numerical integration of ordinary differential equations gives the reaction zone structure. Examples of strong, weak overdriven, and weak underdriven oblique detonations are presented.

Model Equations

We adopt many of the assumptions and nomenclature of Fickett and Davis[8]. The model equations are taken to be the two-dimensional steady Euler and species evolution equations for a reactive calorically perfect ideal gas. These are expressed in dimensionless conservative form:

$$\frac{\partial}{\partial x}\left(\rho u\right) + \frac{\partial}{\partial y}\left(\rho v\right) = 0, \tag{1}$$

$$\frac{\partial}{\partial x}\left(\rho u^2 + P\right) + \frac{\partial}{\partial y}\left(\rho uv\right) = 0, \tag{2}$$

$$\frac{\partial}{\partial x}\left(\rho uv\right) + \frac{\partial}{\partial y}\left(\rho v^2 + P\right) = 0, \tag{3}$$

$$\begin{aligned}\frac{\partial}{\partial x}&\left[\rho u\left(e + 1/2\left(u^2+v^2\right) + P/\rho\right)\right] \\ &+\tfrac{\partial}{\partial y}\left[\rho v\left(e + 1/2\left(u^2+v^2\right) + P/\rho\right)\right] = 0,\end{aligned} \tag{4}$$

$$\frac{\partial}{\partial x}\left(\rho u\lambda_1\right) + \frac{\partial}{\partial y}\left(\rho v\lambda_1\right) = \kappa\rho\left(1-\lambda_1\right)e^{-\epsilon\Theta_1/T}, \tag{5}$$

$$\frac{\partial}{\partial x}\left(\rho u\lambda_2\right) + \frac{\partial}{\partial y}\left(\rho v\lambda_2\right) = \rho\left(\lambda_1-\lambda_2\right)e^{-\epsilon\Theta_2/T}, \tag{6}$$

$$e = \frac{1}{\gamma-1}\frac{P}{\rho} - \epsilon\left(\lambda_1 q_1 + \lambda_2 q_2\right), \tag{7}$$

$$P = \rho T. \tag{8}$$

The variables contained in Eqs. (1–8) are the density ρ, the Cartesian velocity components u and v, the

pressure P, the temperature T, the internal energy e, the reaction progress variables λ_1 and λ_2, and the Cartesian position coordinates x and y. The parameter ϵ is defined as the reciprocal of the square of the freestream Mach number ($\epsilon = 1/{M_0}^2$). Other dimensionless parameters include the ratio of specific heats γ, a kinetic constant κ, the heats of reaction q_1 and q_2, and the activation energies Θ_1 and Θ_2. Equations (1–4) represent the conservation of mass, x-momentum, y-momentum, and energy, respectively. Equations (5–6) are species evolution equations which incorporate an Arrhenius depletion model. Equations (7–8) are caloric and thermal equations of state.

A two-step reaction mechanism is employed, $A \rightarrow B \rightarrow C$, in which the first reaction is exothermic and the second reaction is endothermic. The variables and parameters indicated by the subscripts "1" and "2" correspond to the first and second reaction, respectively. The reaction progress variables λ_1 and λ_2 both range from zero before reaction to unity at complete reaction. Species mass fractions, Y_i, are related to the reaction progress variables by the formulae, $Y_A = 1 - \lambda_1$, $Y_B = \lambda_1 - \lambda_2$, and $Y_C = \lambda_2$. It is convenient to define the dimensionless net chemical heat release Q as a function of the reaction progress variables,

$$Q(\lambda_1, \lambda_2) = \lambda_1 q_1 + \lambda_2 q_2, \tag{9}$$

Initial pre-shock conditions are specified as $\rho = 1$, $u = \sqrt{\gamma}\sin\beta$, $v = \sqrt{\gamma}\cos\beta$, $P = \epsilon$, $\lambda_1 = 0$, and $\lambda_2 = 0$.

Equations (1-8) have been scaled such that in the hypersonic limit ($\epsilon \rightarrow 0$) the post-shock pressure, density, and velocities are all $O(1)$ quantities. The reaction scheme has associated with it two length scales corresponding to the reaction zone lengths of both the exothermic and endothermic reaction. For this analysis, the reaction zone length associated with the endothermic reaction is chosen as the reference length scale. In terms of dimensional variables (indicated by the notation "˜") and dimensional pre-shock ambient conditions (indicated by the subscript "0"), the dimensionless variables are defined by

$$\rho = \frac{\tilde{\rho}}{\tilde{\rho}_0}, \qquad P = \frac{\tilde{P}}{M_0^2 \tilde{P}_0},$$

$$u = \frac{\tilde{u}}{M_0\sqrt{\tilde{P}_0/\tilde{\rho}_0}}, \qquad v = \frac{\tilde{v}}{M_0\sqrt{\tilde{P}_0/\tilde{\rho}_0}},$$

$$x = \frac{\tilde{k}_2\tilde{x}}{M_0\sqrt{\tilde{P}_0/\tilde{\rho}_0}}, \qquad y = \frac{\tilde{k}_2\tilde{y}}{M_0\sqrt{\tilde{P}_0/\tilde{\rho}_0}}. \tag{10}$$

Remaining dimensionless parameters are defined by the following relations:

$$q_1 = \frac{\tilde{\rho}_0\tilde{q}_1}{\tilde{P}_0}, \qquad q_2 = \frac{\tilde{\rho}_0\tilde{q}_2}{\tilde{P}_0}, \qquad \kappa = \frac{\tilde{k}_1}{\tilde{k}_2},$$

$$\Theta_1 = \frac{\tilde{\rho}_0\tilde{E}_1}{\tilde{P}_0}, \qquad \Theta_2 = \frac{\tilde{\rho}_0\tilde{E}_2}{\tilde{P}_0}. \tag{11}$$

Here, $\tilde{E}_1$ and $\tilde{E}_2$ are the dimensional activation energies and $\tilde{k}_1$ and $\tilde{k}_2$ are the kinetic rate constants.

Preliminary Analysis

Equations (1-6) are simplified by assuming there are no changes in the direction tangent to the shock; hence, $\frac{\partial}{\partial y} = 0$. Using the subsequent result that ρu is invariant and eliminating e and T by use of Eqs. (7,8), the system reduces to the following set of ordinary differential equations:

$$\frac{d}{dx}(\rho u) = 0, \tag{12}$$

$$\frac{d}{dx}\left(\rho u^2 + P\right) = 0, \tag{13}$$

$$\frac{dv}{dx} = 0, \tag{14}$$

$$\frac{d}{dx}\left[\left(\frac{1}{\gamma - 1}\frac{P}{\rho} - \epsilon Q\right) + \frac{1}{2}\left(u^2 + v^2\right) + \frac{P}{\rho}\right] = 0, \tag{15}$$

$$\frac{d\lambda_1}{dx} = \kappa\frac{1 - \lambda_1}{u}e^{-\epsilon\Theta_1\rho/P}, \tag{16}$$

$$\frac{d\lambda_2}{dx} = \frac{\lambda_1 - \lambda_2}{u}e^{-\epsilon\Theta_2\rho/P}. \tag{17}$$

Consequences of these assumptions are that u depends only on x, and v is a constant through both the shock and reaction zone; hence, the entire flow field is irrotational.

Using the initial conditions, Eqs. (12-15) can be integrated to yield algebraic RH equations which are valid through both the shock and reaction zone:

$$\rho u = \sqrt{\gamma}\sin\beta, \tag{18}$$

$$\rho u^2 + P = \epsilon + \gamma\sin^2\beta, \tag{19}$$

$$v = \sqrt{\gamma}\cos\beta, \tag{20}$$

$$\left(\frac{1}{\gamma - 1}\frac{P}{\rho} - \epsilon Q\right) + \frac{1}{2}\left(u^2 + \gamma\cos^2\beta\right) + \frac{P}{\rho} = \epsilon\frac{\gamma}{\gamma - 1} + \frac{\gamma}{2}. \tag{21}$$

When $Q(\lambda_1,\lambda_2)=0$, Eqs. (18-21) reduce to standard inert oblique shock equations. This is expected as it can be formally shown from Eqs. (1-8) that through an inert shock, modelled as infinitely thin, reaction has no time to take place, and the jump in reaction progress is zero.

Equations (18,19,21) can be solved for ρ, u, and P as functions of λ_1,λ_2. These relations are presented in a form equivalent to that of Gross[3]:

$$\rho(\lambda_1,\lambda_2)=\left(\frac{1+\gamma\,(1/\epsilon)\sin^2\beta\pm\sqrt{A}}{(\gamma+1)\,(1/\epsilon)\sin^2\beta}\right)^{-1},$$

where

$$A=\left(1+\gamma\,(1/\epsilon)\sin^2\beta\right)^2-(\gamma+1)\,(1/\epsilon)\sin^2\beta \times\left(2+2Q(\lambda_1,\lambda_2)\tfrac{(\gamma-1)}{\gamma}+(\gamma-1)\,(1/\epsilon)\sin^2\beta\right), \tag{22}$$

$$u(\lambda_1,\lambda_2)=\frac{\sqrt{\gamma}\sin\beta}{\rho(\lambda_1,\lambda_2)}, \tag{23}$$

$$P(\lambda_1,\lambda_2)=\epsilon+\gamma\sin^2\beta\left(1-\frac{1}{\rho(\lambda_1,\lambda_2)}\right). \tag{24}$$

For small Q, the "$-$" root of Eq. 22 is a perturbation of the shocked state, and the "+" root is a perturbation of the inert state. The two branches are thus called the shock and inert branches, respectively. In obtaining a weak underdriven detonation solution with a lead shock, we will begin on the shock branch and pass through a critical point to the inert branch.

With the pressure, density, and velocity fields parameterized by λ_1 and λ_2, Eqs. (16,17) can be expressed in the form:

$$\frac{d\lambda_1}{dx}=f_1(\lambda_1,\lambda_2),\qquad \lambda_1(0)=0, \tag{25}$$

$$\frac{d\lambda_2}{dx}=f_2(\lambda_1,\lambda_2),\qquad \lambda_2(0)=0. \tag{26}$$

Equations (25,26) are integrated numerically to find λ_1 and λ_2 as functions of x; thus Q, and subsequently ρ, P, u, e, and T, can be calculated throughout the reaction zone.

Hypersonic Limit

In the hypersonic limit, ($\epsilon\to 0$), a closed form asymptotic solution can be obtained. In this limit the chemical energy release only slightly disturbs the flow, which has a large kinetic energy. Equations (22-24) solved in this limit to $O(\epsilon)$ yield:

$$\rho(\lambda_1,\lambda_2)=\frac{\gamma+1}{\gamma-1} -\epsilon\tfrac{(\gamma+1)^2}{(\gamma-1)\gamma\sin^2\beta}\left(Q(\lambda_1,\lambda_2)+\tfrac{2\gamma}{\gamma^2-1}\right), \tag{27}$$

$$u(\lambda_1,\lambda_2)=\frac{\sqrt{\gamma}(\gamma-1)\sin\beta}{(\gamma+1)} +\epsilon\tfrac{(\gamma-1)}{\sqrt{\gamma}\sin\beta}\left(Q(\lambda_1,\lambda_2)+\tfrac{2\gamma}{\gamma^2-1}\right), \tag{28}$$

$$P(\lambda_1,\lambda_2)=\frac{2\gamma\sin^2\beta}{\gamma+1} -\epsilon\,(\gamma-1)\left(Q(\lambda_1,\lambda_2)+\tfrac{1}{\gamma+1}\right). \tag{29}$$

In Eqs. (16-17) at $O(1)$, the argument of the exponential function is zero, and the velocity u has its constant $O(1)$ post-shock value. Thus these equations may be integrated to give the $O(1)$ reaction zone structure explicitly:

$$\lambda_1=1-exp\left(-\frac{\kappa\,(\gamma+1)\,x}{\sqrt{\gamma}\,(\gamma-1)\sin\beta}\right), \tag{30}$$

$$\lambda_2=1-\left(1+\frac{(\gamma+1)\,x}{\sqrt{\gamma}\,(\gamma-1)\sin\beta}\right) \times exp\left(-\frac{(\gamma+1)\,x}{\sqrt{\gamma}\,(\gamma-1)\sin\beta}\right),\qquad(\kappa=1), \tag{31}$$

$$\lambda_2=1-\left(\frac{\kappa}{\kappa-1}\right)exp\left(-\frac{(\gamma+1)\,x}{\sqrt{\gamma}\,(\gamma-1)\sin\beta}\right) +\left(\frac{1}{\kappa-1}\right)exp\left(-\frac{\kappa\,(\gamma+1)\,x}{\sqrt{\gamma}\,(\gamma-1)\sin\beta}\right),(\kappa\neq 1). \tag{32}$$

When the reaction progress field (30-32) is substituted into Eqs. (27-29), one obtains the pressure, velocity, and density fields to $O(\epsilon)$.

Results

In this section we give results, not restricted to the hypersonic limit, for 1) P,λ_1 phase portraits for several values of β and their relation to oblique detonation polars, 2) streamlines and characteristics, 3,4,5) an example of oblique detonation structure for each solution class: **I**, strong, **II**, weak overdriven, and **III**, weak underdriven, and 6) an illustration of the behavior of the weak underdriven solution as the endothermicity (q_2) is reduced to 0 with the net complete reaction heat release, $Q(1,1)$, held constant.

In all examples considered [except 6), which considers the relative endothermicity] we take $\epsilon=1/100$ (so that the incoming Mach number is 10), $\gamma=7/5$, $\kappa=1$, $\Theta_1=\Theta_2=0$, $q_1=100$, and $q_2=-75$. For Case **I** we take a representative angle, $\beta=80°$. For Case **II** we take a representative angle, $\beta=60°$. For Case **III** an eigenvalue wave angle is found to be

$\beta = \tilde{\beta} = 52.77°$. For these three cases, the respective labels **I**, **II**, and **III** are adopted. Phase portraits are also presented at the detachment wave angle for this system, $\beta = \beta_{detach} = 65.65°$, at the subsonic to supersonic transition wave angle, $\beta = \beta_{SS} = 65.53°$, for a representative shockless structure with turning angle $\beta = 60°$, and for a representative structure for which imaginary solutions are obtained, $\beta = 50°$.

Phase Space Portraits and Detonation Polars

Equations (25,26) were integrated numerically using a Runge-Kutta technique. Results are summarized in the P, λ_1 phase plane shown in Fig. 3. The variables ρ, P, and u for structures with a lead shock are calculated using the shock branch of Eq. (22). The flow is shocked from the inert state at **O** to the Neumann point **N**. For strong solutions such as **I**, where $\beta_{detach} < \beta \leq 90°$, as the reaction progresses, the pressure decreases from its value at **N** to a pressure minimum and then increases to its final value at the strong point **S**. The phase space trajectories are topologically equivalent for weak overdriven solutions such as **II**, for both $\beta_{SS} < \beta \leq \beta_{detach}$ and $\tilde{\beta} < \beta \leq \beta_{SS}$. In such cases the trajectory begins at **O**, is shocked to **N**, and terminates at **WO**. There is also nothing topological to distinguish the trajectories at either $\beta = \beta_{detach}$ or $\beta = \beta_{SS}$, which are also plotted in Fig. 3. As the difference between β_{detach} and β_{SS} is very small, the difference in the two trajectories has been slightly exaggerated so they can be distinguished on this scale.

The **I** trajectory, $\mathbf{O} - \mathbf{N} - \mathbf{S}$, and **II** trajectory, $\mathbf{O} - \mathbf{N} - \mathbf{WO}$, are also plotted in β, θ space on the polars of Fig. 4. On each trajectory the fluid reacts with the exothermic reaction dominant until the heat release reaches a local maximum, Q_{max} at which point the endothermic reaction dominates until complete reaction when $Q = 25$. In these and all cases studied, Q_{max} was nearly constant at 44.8.

The behavior of the P, λ_1 trajectories can be predicted by using Eqs. (12-17) to explicitly solve for the pressure derivative:

$$\frac{dP}{dx} = \epsilon \frac{(\gamma - 1)\,\rho u^2 \left(q_1 \frac{d\lambda_1}{dx} + q_2 \frac{d\lambda_2}{dx}\right)}{u^2 - \gamma(P/\rho)}. \qquad (33)$$

Using Eqs. (22-24) to evaluate ρ, u, and P downstream of the shock along with Eqs. (16,17) to evaluate reaction progress derivatives, it is easily shown that just past the shock, $\frac{dP}{dx} < 0$. It is also seen that $u > 0$; thus, from Eq. (16), it is deduced that λ_1 is a monotonically increasing function of x. Thus, pressure variations with x and λ_1 are qualitatively similar. The predicted pressure minimum is a consequence of the quantity $q_1 \frac{d\lambda_1}{dx} + q_2 \frac{d\lambda_2}{dx} = \frac{dQ}{dx}$ reaching zero at an interior point of the reaction zone. As the reaction progress derivatives for the irreversible reaction scheme are always positive; this zero can only be reached if one reaction is exothermic and the other endothermic.

As β is reduced from 90°, it is possible to predict a continuum of strong solutions until $\beta = \beta_{detach}$ and a continuum of weak overdriven solutions from $\beta = \beta_{detach}$ until a certain eigenvalue wave angle $\beta = \tilde{\beta}$ is reached. At $\beta = \tilde{\beta}$, the solution trajectories reach a saddle critical point, labelled **P** for pathological, in P, λ_1 phase space. At **P**, $\frac{dQ}{dx}$ and $u^2 - \gamma P/\rho$ are simultaneously zero; i. e. the heat release rate approaches zero as the local Mach number approaches unity. It is also seen that the quantity A in Eq. (22) is simultaneously zero. Thus, integration can be continued on either the shock or inert branch of Eq. (22). Integration along the shock branch carries the trajectory to a final weak overdriven state **WO**, while if the inert branch is selected, the solution proceeds to completion to the weak underdriven point **WU**. The **III** trajectory, $\mathbf{O} - \mathbf{N} - \mathbf{P} - \mathbf{WU}$, is plotted in Figs. 3,4.

For solutions with $\beta > \tilde{\beta}$ which remain on the inert branch, a complementary family of solutions exists. One such trajectory from **O** to **WU** is shown in Fig. 3. The physical justification for the unshocked solution is not clear-cut as there is no distinct initiation mechanism and the equations are subject to the cold boundary difficulty.

For $\beta < \tilde{\beta}$, there is no solution which remains real for $0 \leq \lambda_{1,2} \leq 1$. In P, λ_1 phase space, one family of trajectories is in the neighborhood near $\lambda_1 = 0$. These trajectories originate at **N** or **O** and progress to a termination point **T** where the flow reaches a local sonic state at a point where the heat release rate $\frac{dQ}{dx}$ is non-zero. A complementary family of trajectories exists in the neighborhood of $\lambda_1 = 1$. These originate at the complementary **T** and terminate at either **WO** or **WU**. For the parameters of these example problems, $\beta_{CJ} = 37.02° < \tilde{\beta}$; consequently, there is no real CJ solution.

Streamlines and Characteristics

It is easily shown that the standard expressions for streamlines and characteristics for two-dimensional steady compressible flow, such as those given by Shapiro[9], also apply to this reactive flow field. The family of streamlines $y_s(x)$ and characteristics $y_\pm(x)$ are generated from the known field variables by the

following expressions:

$$y_s(x) = \sqrt{\gamma}\cos\beta \int_{x_o}^{x} \frac{d\check{x}}{u(\check{x})}, \tag{34}$$

$$y_{\pm}(x) = \int_{x_o}^{x} \frac{\sqrt{\gamma}\cos\beta u(\check{x})/a^2(\check{x}) \pm \sqrt{M^2(\check{x})-1}}{M_x^2(\check{x})-1}\, d\check{x},$$

with

$$a^2(x) = \gamma\frac{P(x)}{\rho(x)}, \qquad M_x^2(x) = \frac{u^2(x)}{a^2(x)},$$

$$M^2(x) = \frac{u^2(x)+\gamma\cos^2\beta}{a^2(x)}. \tag{35}$$

Here $\check{x}$ is a dummy variable; x_o gives the initial x position of a particular streamline or characteristic; a is the local sound speed; M is the total local Mach number; and M_x is the local Mach number in the direction normal to the shock. The streamline for $x_0 = 0$ is taken to be coincident with a solid curved wedge which supports the oblique detonation. It is noted that the characteristics are real when $M > 1$ and that the characteristics are parallel to the shock when $M_x = 1$.

In the following examples, **I**, **II**, and **III**, we will plot the streamlines and characteristics in the $(\hat{x}, \hat{y})$ orthogonal coordinate system, which is defined to be aligned with the incoming flow. The appropriate transformations for this system are $\hat{x} = x\sin\beta + y\cos\beta$, and $\hat{y} = -x\cos\beta + y\sin\beta$.

Strong, Case **I**

We give an example of a strong oblique detonation in which $\beta = 80°$. For this case, $M < 1$ and $M_x < 1$ throughout the reaction zone. Reaction zone profiles for reaction progress, λ_1, λ_2, and pressure, P, predicted by both the numerical and asymptotic methods are shown in Figs. 5a,b. The asymptotic and numerical predictions are in quantitative agreement to $O(\epsilon)$. Since $M < 1$, the steady flow field is elliptic, there are no real characteristics, and disturbances at any location are propagated to the entire flow field. The domain of dependency for any point on the shock is the entire region between the shock and the wedge. The streamlines for the strong solution are shown in Figure 5c.

Weak Overdriven, Case **II**

We next consider a weak overdriven oblique detonation in which $\beta = 60°$. In this case, $M > 1$ while $M_x < 1$ throughout the reaction zone. Figures 6a,b,c show the reaction zone profiles for λ_1, λ_2, and P, streamlines and characteristics, respectively. Again numerical and asymptotic predictions are in quantitative agreement to $O(\epsilon)$ and are qualitatively similar to those corresponding to the strong oblique detonation case. All characteristics of the "$-$" family which originate on the wedge surface intersect the shock at a downstream location. The domain of dependency for a given point on the shock is limited to points upstream of the "$-$" characteristic which intersect this point.

Weak Underdriven, Case **III**

We finally consider a weak underdriven (eigenvalue) oblique detonation, which for the parameters of this study occurs at $\beta = \tilde{\beta} = 52.77°$. In this case, $M > 1$, while M_x is subsonic near the shock and supersonic downstream of the shock. Figures 7a,b,c show the reaction zone profiles for λ_1, λ_2, and P, streamlines and characteristics, respectively. For small x the structure is similar to the weak overdriven structure. Upon reaching the pathological point **P**, the structure changes dramatically. The pressure P does not reach a local minimum but monotonically decreases to its value at complete reaction. The streamlines behave similarly to those of the previous two cases.

The characteristics behave much differently. Characteristics of the "$-$" family which originate at the wedge surface near the wedge tip intersect the shock. At a critical location on the wedge surface, which occurs when $M_x = 1$, the "$-$" characteristic is parallel to the lead shock. Characteristics which originate on the wedge surface past this point do not intersect the lead shock. Thus the domain of dependency for any point on the shock is limited to a finite width zone near the shock and is upstream of a given "$-$" characteristic.

Effects of Decreasing Endothermicity

Fig. 8 demonstrates the effect of relative endothermicity on the eigenvalue wave angle $\tilde{\beta}$. To obtain this plot, we simultaneously lower the magnitude of both q_1 and q_2 such that the global heat release at complete reaction is maintained at $Q(1,1) = 25$. As q_2 is lowered, $\tilde{\beta}$ decreases. When $q_2 = 0$, the point **P** becomes coincident with the CJ point, and $\tilde{\beta} = \beta_{CJ} = 37.02°$. Thus as $q_2 \to 0$, for oblique detonations with a lead shock, the model only predicts strong, weak overdriven, and CJ solutions. This result is consistent with the results obtained in Ref. 7.

Final Remarks

This study has demonstrated the critical role that the kinetic scheme can play in determining admissible oblique detonation structures. For the kinetic scheme of this study, the CJ state has relatively little significance. It provides only an overly conservative lower bound for the wave angle, with the true boundary more restrictive. One can induce for reaction schemes with more complex kinetics that the necessary conditions for admissible solutions become correspondingly more complex.

Though the flow physics are different, these oblique detonation flows have a remarkably similar mathematical structure as such classical flows[9] as 1) one-dimensional Rayleigh flow, or 2) one-dimensional inert flow with area change. For instance, the pathological point **P** of this study is analogous to a one-dimensional inert flow simultaneously reaching an area minimum and a local sonic state. Since the one-dimensional inert flow is able to relax to a variety of downstream boundary conditions when one allows a normal shock to stand in the duct, we hypothesize that there is a wider range of oblique detonation solutions available when one allows for multiple shock structures.

The question of the structural, numerical, and hydrodynamic stability of these waves is open to question. We consider a solution to be *structurally stable* if a small change in any parameter results in a small change in the steady flow field without any regard to time-dependent phenomena. We consider a solution to be *numerically stable* if a particular numerical method tends to converge to the steady solution. We consider a solution to be *hydrodynamically stable* if any disturbance which is imposed for a finite time tends to decay so as to return the system to its original state.

Powers and Stewart[7] have given an example of the structural stability of irrotational weak overdriven oblique detonations. They showed straightening the curved wedge only changes the flow field by introducing a small amount of vorticity near the wedge surface and that far from the wedge, the solution remains the same, with a straight shock and curved streamlines. It is hypothesized that since the weak overdriven solutions of this study are perturbations of those of Ref. 7, that these too would be structurally stable to changes in the wedge shape. The weak underdriven case presented here is structurally unstable. Any parametric change would result in no steady solution. The weak underdriven solution may still be of value, however, if for instance 1) the solution is a degenerate case of a solution with a more complicated shock structure, or 2) effects not modelled here, such as diffusive transport effects, have the consequence of being stabilizing influences.

Powers and Grismer[10] have shown the the oblique detonations of Ref. 7 are numerically stable for one particular numerical method. Again, it is believed that the weak overdriven solutions of this study should also be numerically stable.

The hydrodynamic stability of all solution classes remains an open question.

Acknowledgments

This study was sponsored by the 1991 NASA-ASEE Summer Faculty Fellowship Program and the University of Notre Dame. A portion of this work was conducted during the authors' residence at the NASA Lewis Research Center.

References

[1]Siestrunck, R., Fabri, J., and Le Grivès, E., "Some Properties of Stationary Detonation Waves," *Proceedings of the Fourth Symposium (International) on Combustion*, Williams and Wilkins, Baltimore, MD, 1953, pp. 498-501.

[2]Gross, R. A., and Chinitz, W., "A Study of Supersonic Combustion," *Journal of the Aero/Space Sciences*, Vol. 27, No. 7, 1960, pp. 517-524.

[3]Gross, R. A., "Oblique Detonation Waves," *AIAA Journal*, Vol. 1, No. 5, 1963, pp. 1225-1227.

[4]Oppenheim, A. K., Smolen, J. J., and Zajac, L. J., "Vector Polar Method for the Analysis of Wave Intersections," *Combustion and Flame*, Vol. 12, No. 1, 1968, pp. 63-76.

[5]Chernyi, G. G., "Supersonic Flow Past Bodies with Formation of Detonation and Combustion Fronts," *Problems of Hydrodynamics and Continuum Mechanics*, English Edition, SIAM, Philadelphia, PA, 1969, pp. 145-169.

[6]Pratt, D. T., Humphrey, J. W., and Glenn, D. E., "Morphology of a Standing Oblique Detonation Wave," AIAA Paper 87-1785, 1987.

[7]Powers, J. M., and Stewart, D. S., "Approximate Solutions for Oblique Detonations in the Hypersonic Limit," to appear in the *AIAA Journal*.

[8]Fickett, W., and Davis, W. C., *Detonation*, Univ. California Press, Berkeley, 1979.

[9]Shapiro, A. H., *The Dynamics and Thermodynamics of Compressible Fluid Flow, Volume I*, John Wiley, New York, 1953.

[10]Powers, J. M., and Grismer, M. J., "Comparisons of Numerical and Exact Solutions for Oblique Detonations with Structure," AIAA Paper 91-1677, 1991.

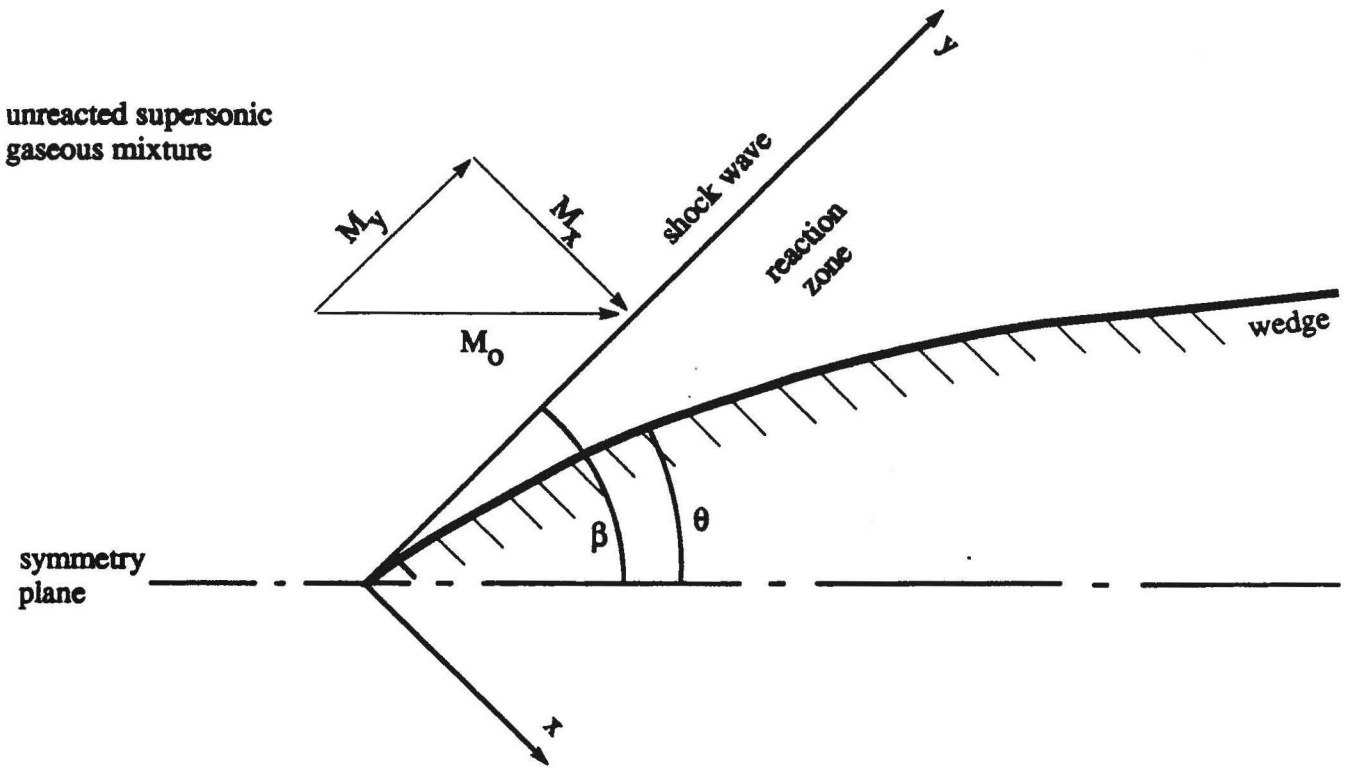

Figure 1. Schematic of oblique detonation with a straight shock attached to a curved wedge.

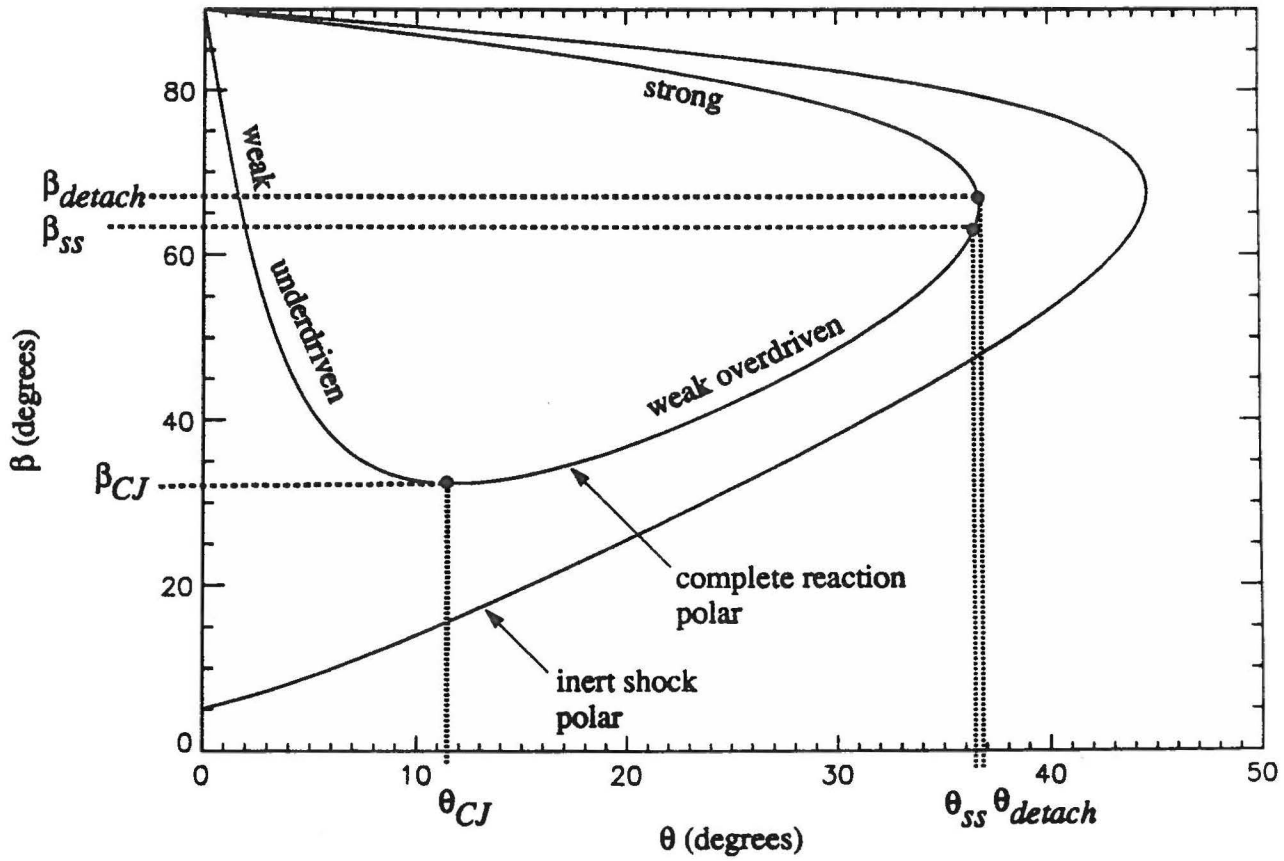

Figure 2. Inert [Q(0,0) = 0] and complete reaction [Q(1,1) = 25] polars (M_o = 10, γ = 7/5).

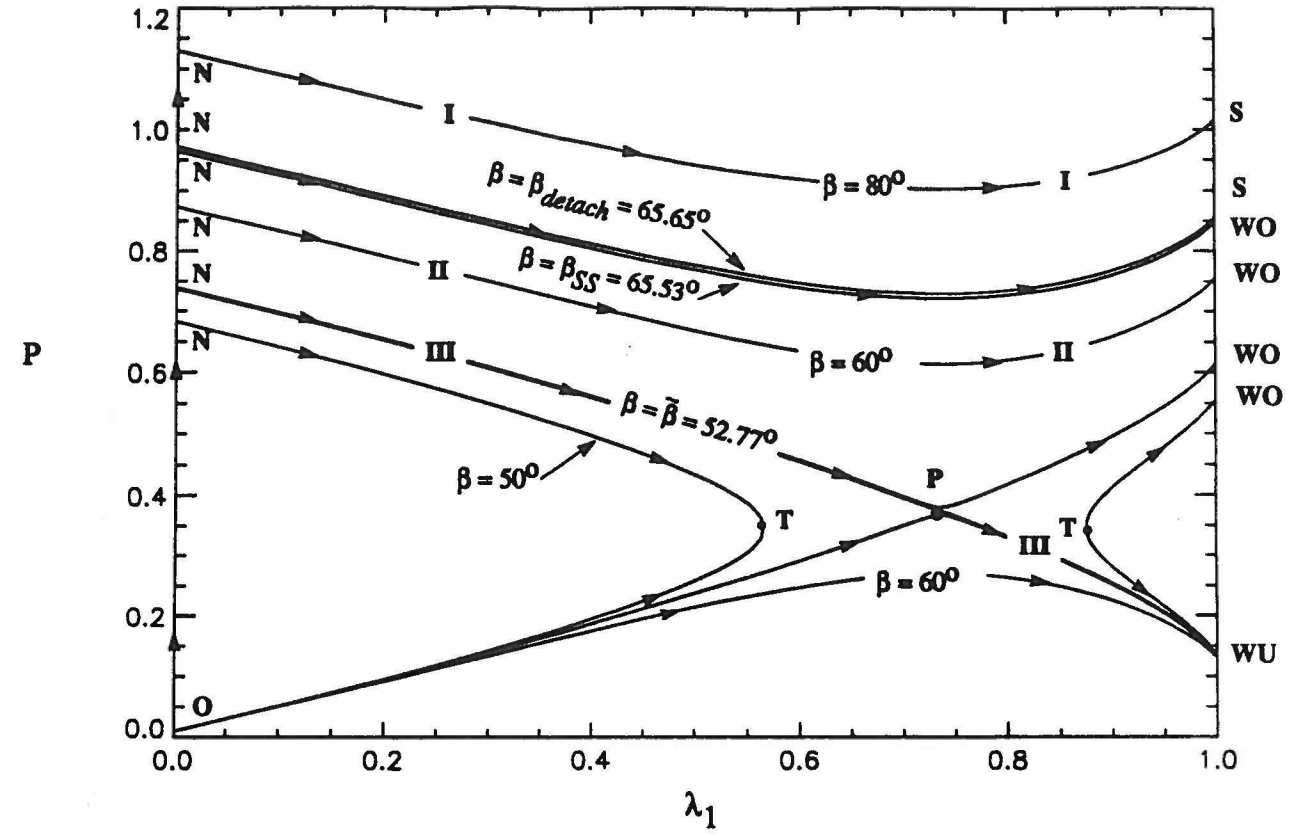

Figure 3. P, λ_1 phase plane.

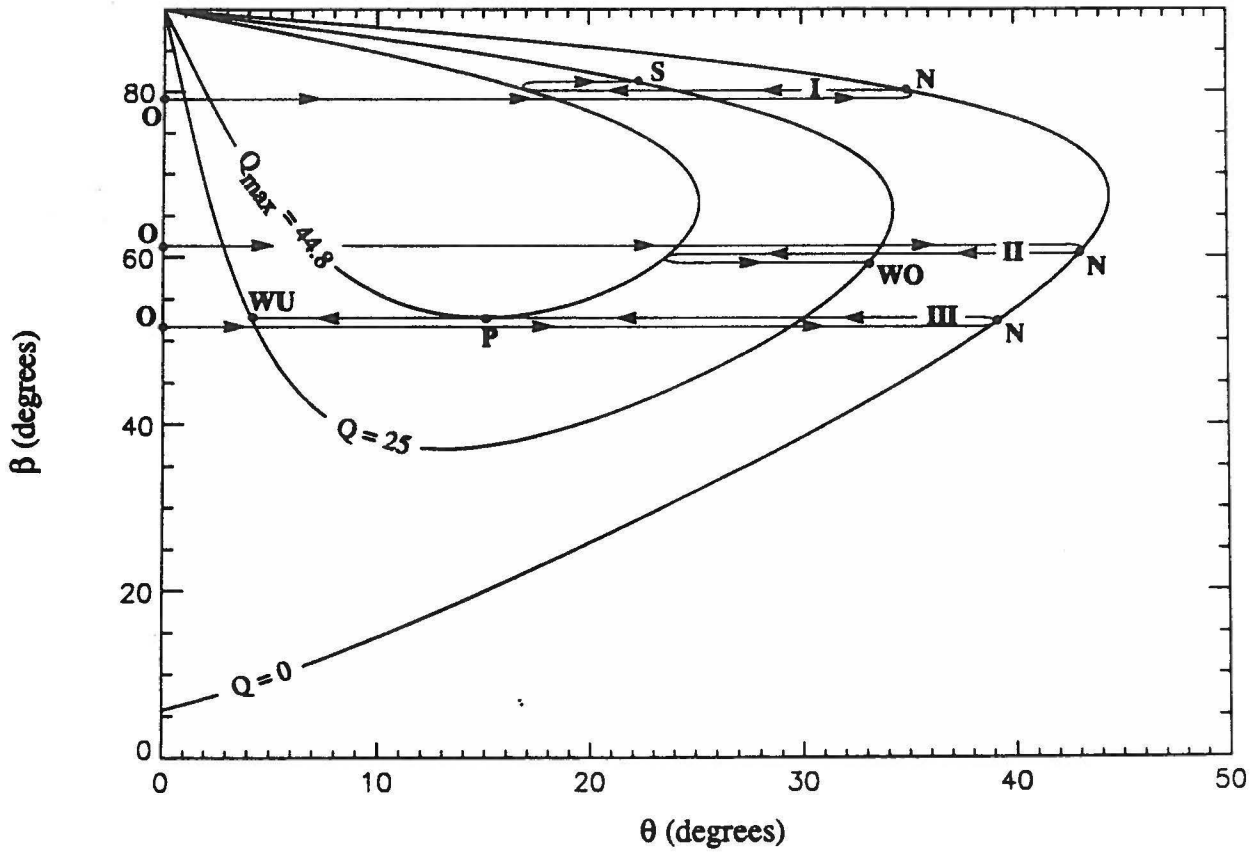

Figure 4. Inert, intermediate, and complete reaction shock polars.

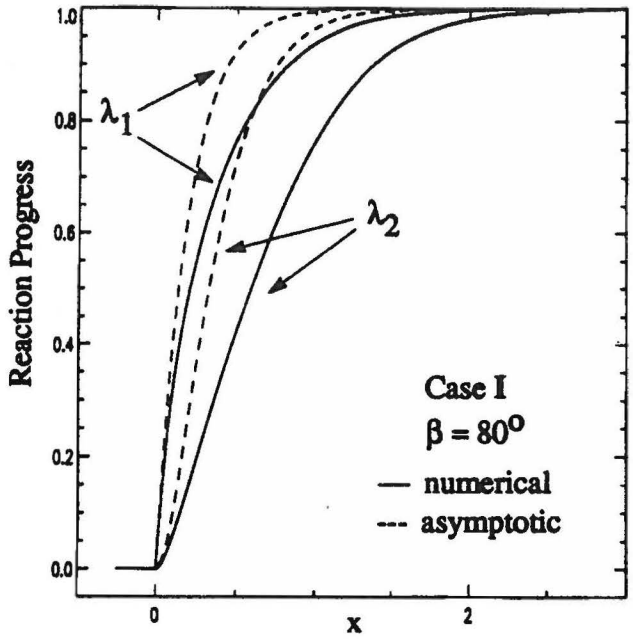

Figure 5a. Predictions of the reaction progress variables for a strong oblique detonation.

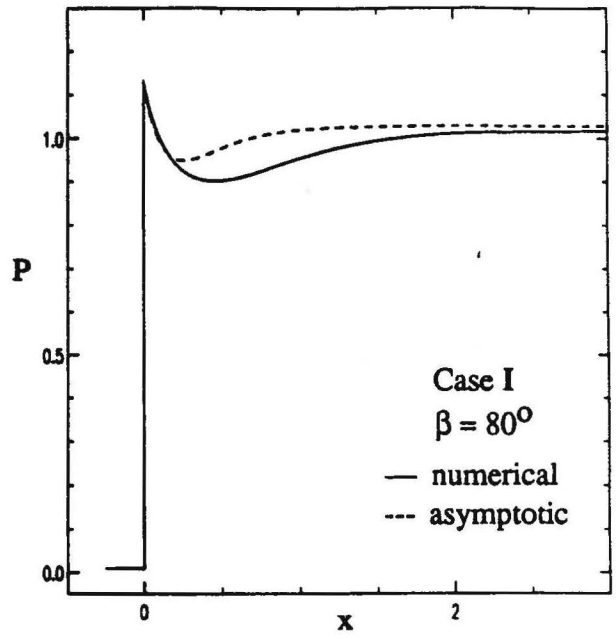

Figure 5b. Predictions of pressure for a strong oblique detonation.

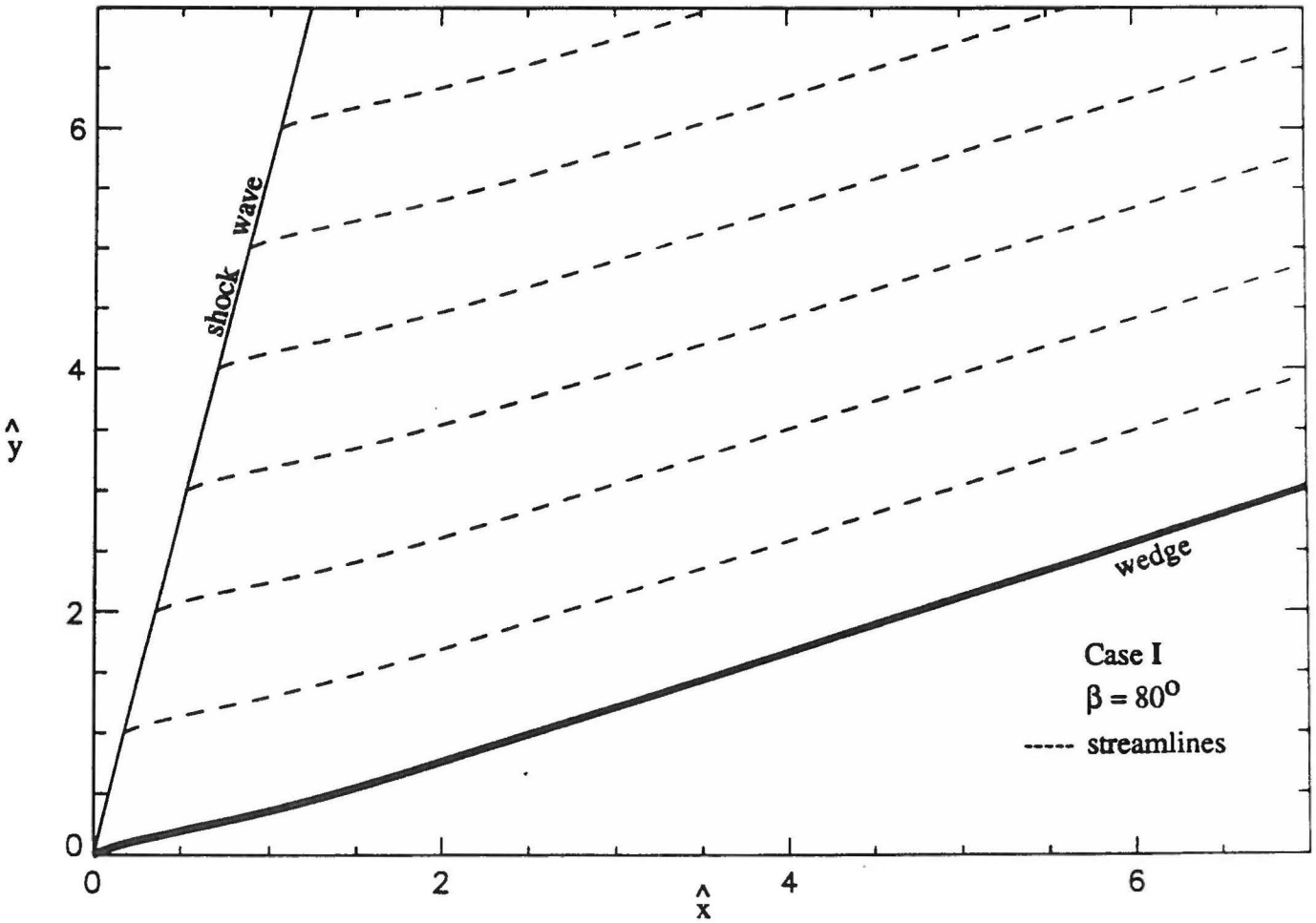

Figure 5c. Streamlines for a strong oblique detonation.

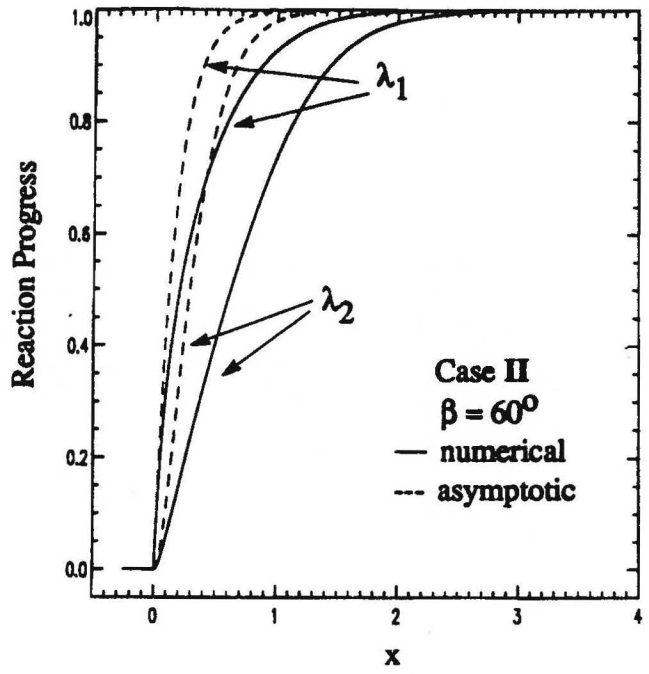

Figure 6a. Predictions of the reaction progress variables for a weak overdriven oblique detonation.

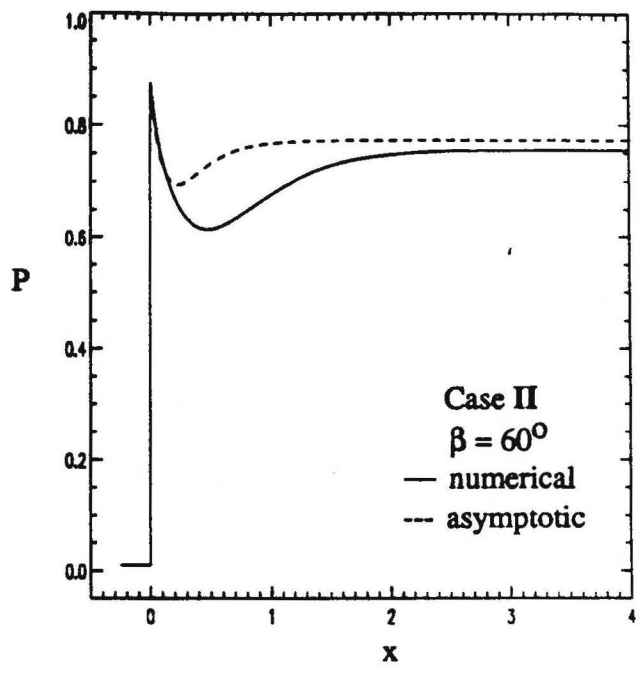

Figure 6b. Predictions of pressure for a weak overdriven oblique detonation.

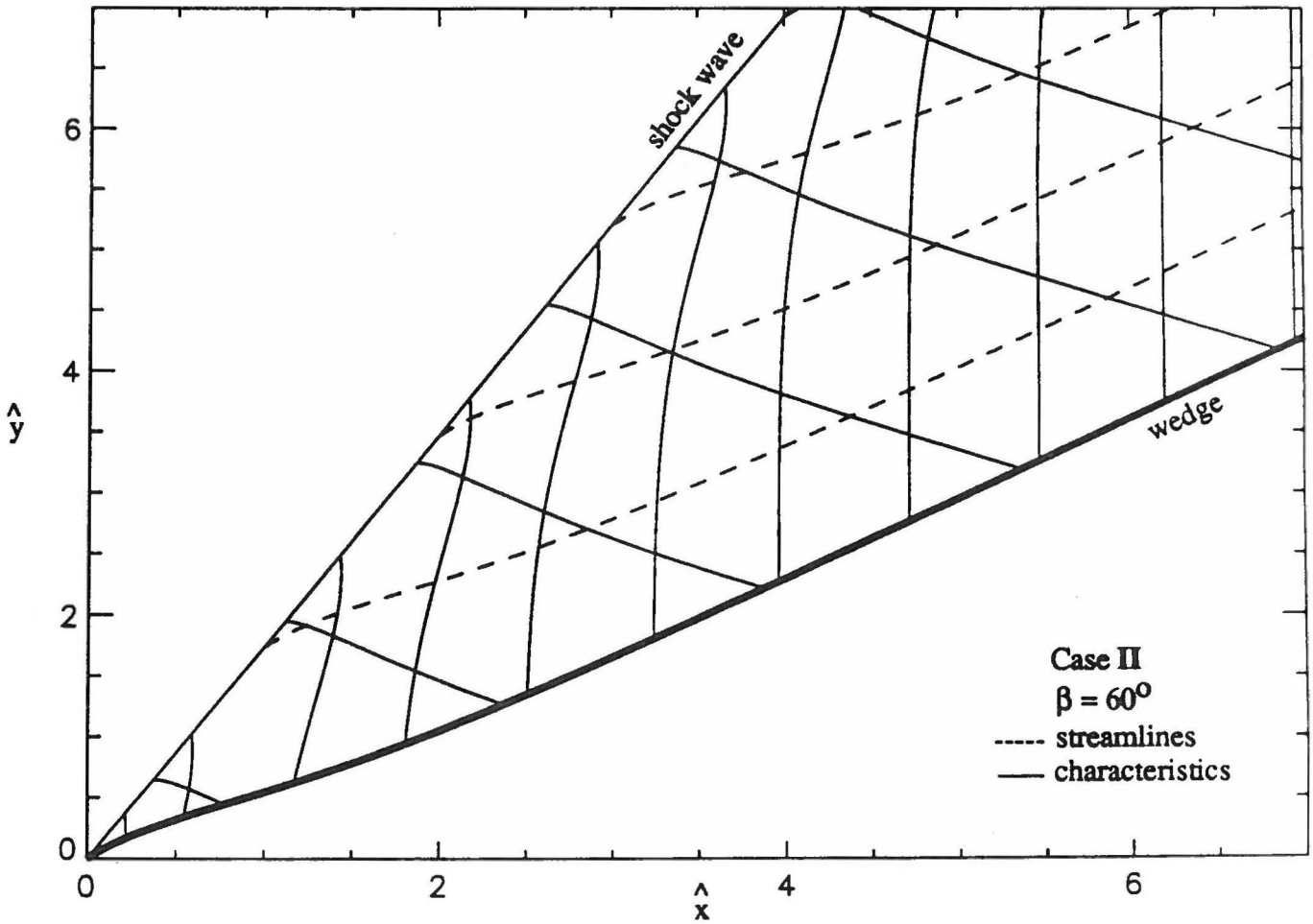

Figure 6c. Streamlines and characteristics for a weak overdriven oblique detonation.

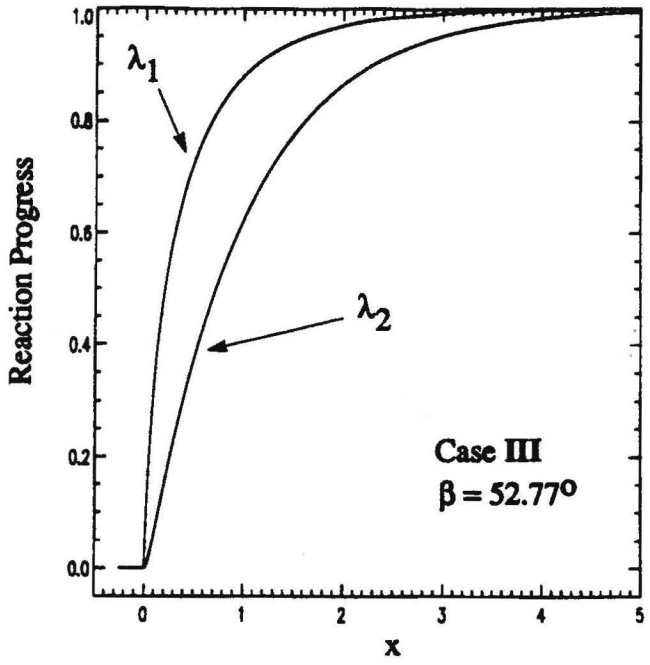

Figure 7a. Numerical prediction of the reaction progress variables for the weak underdriven oblique detonation.

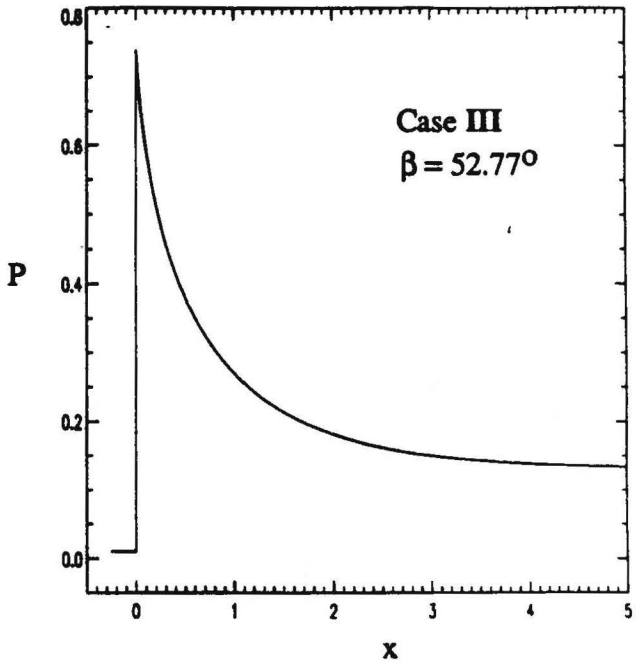

Figure 7b. Numerical predictions of pressure for the weak underdriven oblique detonation.

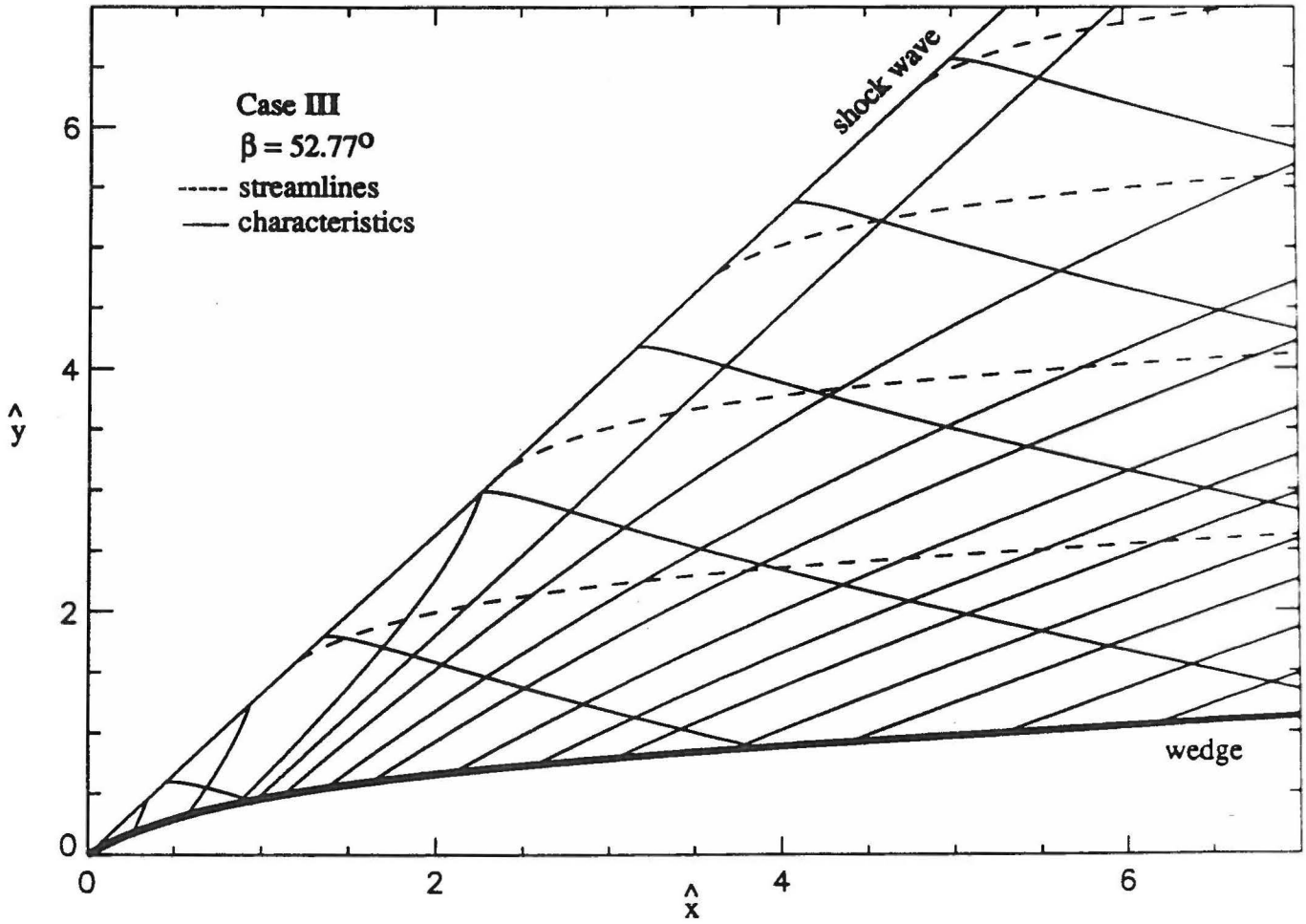

Figure 7c. Streamlines and characteristics for the weak underdriven oblique detonation.

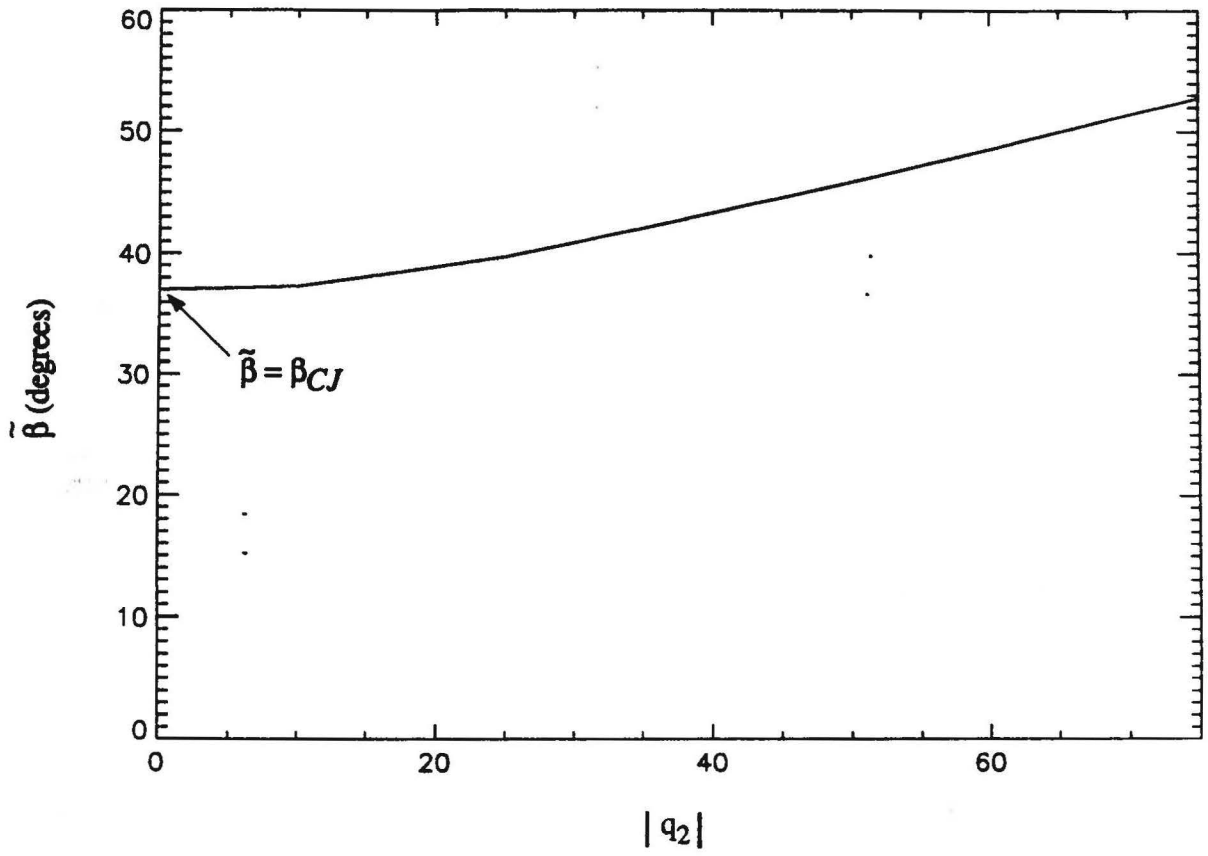

Figure 8. Eigenvalue wave angle $\tilde{\beta}$ as a function of endothermicity q_2.